

# Comparative magnetic analysis of I-type actuator based active magnetic bearing system

Sukanta Debnath \*, Pabitra Kumar Biswas †

## Abstract

We investigated the performance of designed single coil and multi-coil actuators for the Active Magnetic Bearing (AMB) system. The attractive force differs depending on the structure and actuator design. The behavior and characteristics of particular actuators differ too. Ansys Maxwell was used to perform magnetic analyses of flux, flux density, field strength, force profile and inductance profile in 2D, and magnetic flux density, field strength, current density and inductance profile in 3D. These analyses were performed for the 10 mm air gap between the actuator and rotor for single, two, three and four coils and all the parameters were compared. The quantities were compared to provide insight into the behavior of single and multi-coil actuators.

**Keywords:** active magnetic bearing, Ansys Maxwell, I-type actuator, Magnetic analysis, Matlab

## 1 Introduction

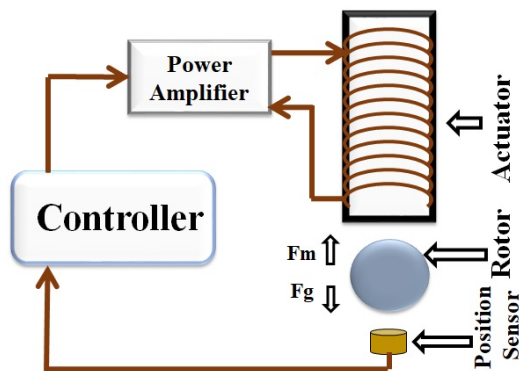


Figure 1: Block diagram of AMB

AMB has multiple applications in industry, like drive systems, high speed machineries, renewable energy, space etc. The many advantages of this type of bearing include: no friction, lower power consumption and high speed through the lack of contact between stator and rotor. The AMB system has four parts: actuator

and rotor, sensor, power amplifier and controller, as shown in Fig. 1 [1]; [2].

The actuator is the most important part of the AMB system. The performance of the proposed system depends on the position between the actuator and rotor [3]. Ansys Maxwell based software was used to investigate and analyze the actuator [4]; [5]. Depending on the application, various types of AMB were considered: single coil, double coil, triple coil and quadruple coil. Schematic diagrams of single and multi-coil AMBs are shown in Fig. 2. Analysis is performed for all four types of actuator with rotor for AMB in 2D and 3D [6]; [7].

Extensive magnetic analysis was conducted for different air gaps between actuator and rotor. By increasing the air gap all the parameters decrease. Single coil and triple coil I-type actuator force is greater than for the double and quadruple coil, because there is no opposition force [8]; [9].

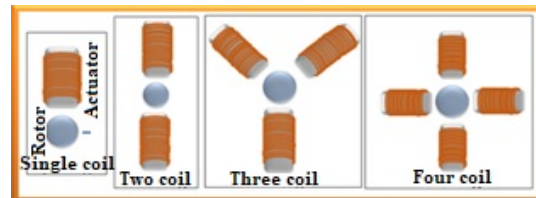


Figure 2: Schematic diagram of single and multi-coil actuators for AMB

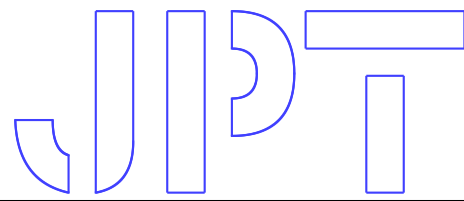
In this paper analysis of an I-type actuator is performed in 2D for flux lines, flux density, field intensity, force and inductance and the results compared for single and multi-coil and 3D analysis for flux density, field intensity and current density [10]. 3D and 2D results are compared for flux density, field strength and inductance profile [6]; [11]; [12]; [13]; [14]; [15].

## 2 Mathematical model of AMB

Due to the triggering current moving through the winding, attractive power is generated as indicated by the Ampere circuit law, the relationship between

\*NIT Mizoram e-mail

†NIT Mizoram e-mail



the current sum included in the integral path and the magnetic field [11] is given by:

$$\oint H \cdot dl = NI \quad (1)$$

where  $N$  is the number of coils turns and  $I$  is the current through the coil. The magnetic flux density is given by:

$$B = \mu_0 \mu_r H \quad (2)$$

Here,  $\mu_r$  is the iron core relative permeability and  $\mu_0$  is the relative permeability of air. Ferromagnetic material is fairly permeable as long as the magnetic flux is stable, and the cross sectional spectrum and air distance are assumed to be equivalent [16]. Therefore,

$$\phi_s = B_s A_s = B_A A_A = \frac{\mu_0 I}{2z} n A_A \quad (3)$$

Therefore,

$$B_s = B_A = B \quad (4)$$

The magnetic route is divided into two parts, the magnetic field in the air and the magnetic material.

$$nI = H_s L_s + 2H_A z \quad (5)$$

From the above equation  $n$  is the average magnetic path length and  $z$  is the air-gap. From Eq. 3 and Eq. 5 the equation of flux density is composed as:

$$B = \frac{\phi}{A_A} \mu_0 \frac{nI}{\frac{L_s}{\mu_r} + 2z} \quad (6)$$

Given relative permeability, the above expression is expressed as:

$$B \approx \frac{nI}{2z} \quad (7)$$

The electromagnetic actuators are only capable of generating attracting forces. The force created by a single-sided magnetic actuator as shown in Fig. 3 is a function of flux density ( $F$ ):

$$F = \frac{B_A^2 A_A}{\mu_0} \quad (8)$$

If the angle between the center of the cross-sectional area and the force direction is  $\theta$ , then using Eq. 6 and Eq. 7 the force equation is communicated as:

$$F = \frac{\mu_0 I^2}{2z^2} n^2 A_A \cos\theta [\theta = 0] \quad (9)$$

In the case of a single actuator  $\cos\theta = 1$ . Therefore, the above expression is given as:

$$F = \frac{\mu_0 I^2}{2z^2} n^2 A_A \quad (10)$$

The above equation refers to a perfect, leakage-free magnetic bearing in the flux path [8]. To reflect the reduction in total force of the magnetic actuator due to fringing and leakage effects it is often suggested that a specific correction factor be incorporated in the force equation :

$$F = \frac{\epsilon_r \mu_0 I^2}{2z^2} n^2 A_A \quad (11)$$

Inductance of an Active Magnetic Bearing is given as:

$$L_m = \frac{n\phi}{I} \quad (12)$$

From Eq. 3, Eq. 5 and Eq. 9, a new expression of inductance is composed:

$$B = N^2 \mu_0 A_A \frac{1}{\frac{L_s}{\mu_0} + 2z} \quad (13)$$

### 3 Design and Simulation of single and multi-coil AMB

The designed model of I-type active magnetic bearing data is given in Table 1 and Table 2, there are set key assumptions, the type of task is determined as is the boundary condition, the geometry of I-type 2D model is shown in Fig. 3(a); also determined are the flux pattern, flux density, field intensity, magnetic force and inductance during the simulation. Since the I-type model is essentially three-dimensional, its three-dimensional designed model is shown in Fig. 3(b) and design data are given in Table 3.

Key assumptions in the simulation of the magnetic field:

Magnetic properties of iron

The geometry of the proposed system the magneto-static field is considered as two-dimensional and three-dimensional.

Table 1: Properties of materials used in ANSYS Maxwell 2D and 3D

Particulars	Rotor (iron)	Actuator (iron)	Coil (copper)	Units
Relative Permeability	4000	10000	0.99	
Bulk Conductivity	103000	103000	580000	s/m
Thermal Conductivity	89	89	400	w/mC

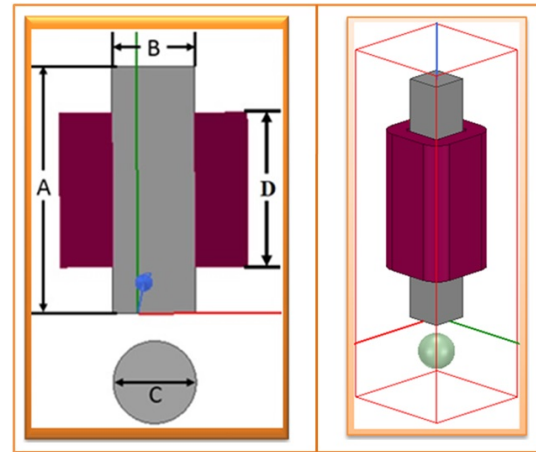


Table 2: Designed model data of I-type core and rotor in ANSYS Maxwell 2D

Parameters	Specification
A	14 cm
B	3 cm
C	3 cm
D	10 cm
Number of turns	700
Currents	4 A
Boundary condition	10%

Figure 3: (a) 2D model of I-type actuator (b) 3D model of I-type actuator

Current density in the winding cross-section is uniformly distributed, coil current is constant.

Boundary condition

Using Maxwell's equation, the static magnetic field problem can be defined. Maxwell's equations in differential form are:

$$\nabla \times D = \rho_v \tag{14}$$

$$\nabla \times H = -\frac{\delta B}{\delta t} \tag{15}$$

$$\nabla \times H = J + \frac{\delta D}{\delta t} \tag{16}$$

Table 3: Designed model data of I-type core and rotor in ANSYS Maxwell 3D

Parameters	Specification
Thickness of the actuator	3 cm <sup>2</sup>
Length of the actuator	14 cm
Thickness of the coil	0.5 cm <sup>2</sup>
Length of the coil	10 cm
Number of turns	700
Currents	4 A
Boundary condition	10%

For static magnetic field  $\frac{\delta D}{\delta t} = 0$ . So,  $\nabla \times H = J$  and  $\nabla \times B = 0$

$$B = \mu H = H \mu_0 \mu_r \tag{17}$$

where H is magnetic field intensity, B is magnetic flux density, J is current density,  $\mu_r$  is the relative permeability of material and  $\mu_0$  is the relative permeability of air.

The structure of the single coil I-type actuator is presented in Fig. 3. For detailed examination of the AMB system current density need to be very. It is known that current density (J) is the ratio of number of coil turns (N), current (I) and coil area. By changing the coil turns current density can be increased or decreased. Iron is used as an actuator material and copper is used for the winding.

The analysis is performed for ten air gaps, from 2mm to 20mm with a step of 2mm for single, double, triple and quadruple coil actuator with rotor. ANSYS Maxwell 17.1 modeling software is used to evaluate different data. The vector plot of the flux pattern in 2D for the 10mm air gap is shown in Figs. 4(a-d), field strength for all four coil actuators is shown in Figs. 5(a-d). Flux density and attraction force for 2D are shown in Figs. 7(a-d) and Figs. 9(a-d). The 3D analysis results of all four coil actuators for field strength, flux density and current density are shown in Figs. 6(a-d), Figs. 8(a-b) and Figs. 10(a-b) respectively.

The analyses show that the flux, field strength, flux density, force and inductance are greater for the single coil actuator than for the double and quadruple coil.

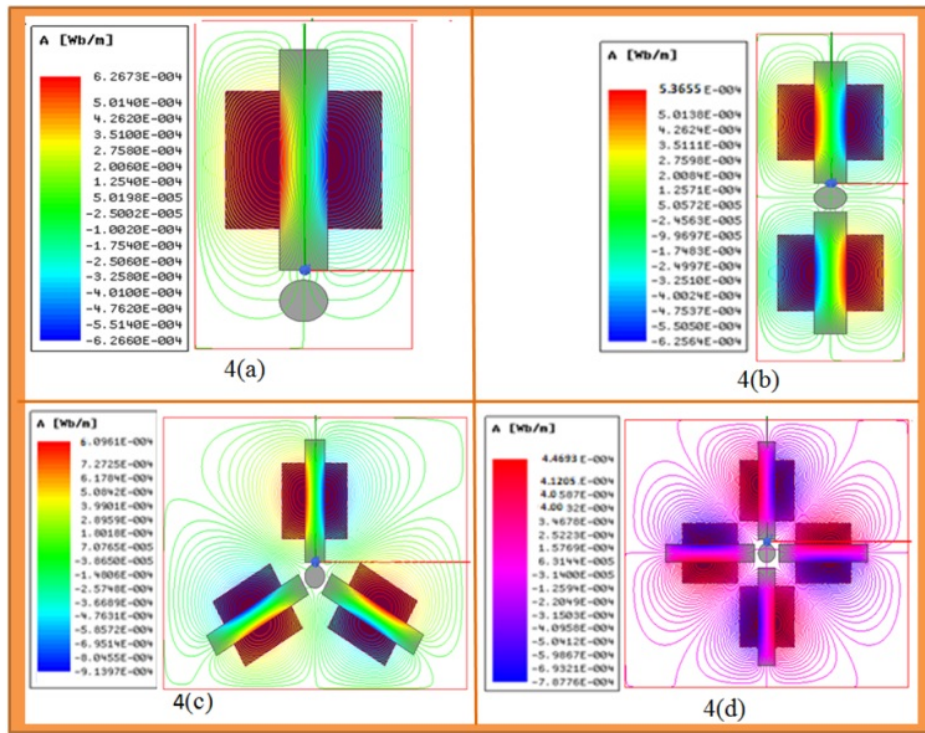


Figure 4: (a) Flux pattern of single coil AMB in 2D (b) Flux pattern of double coil AMB in 2D (c) Flux pattern of triple coil AMB in 2D (d) Flux pattern of quadruple coil AMB in 2D

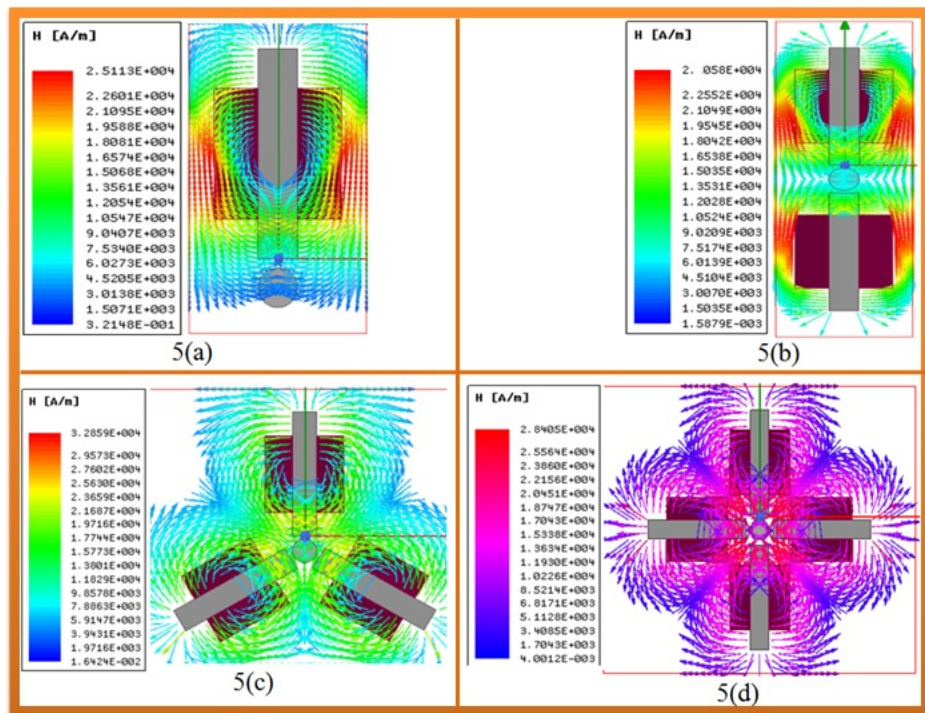


Figure 5: (a) Field strength of single coil AMB in 2D (b) Field strength of double coil AMB in 2D (c) Field strength of triple coil AMB in 2D (d) Field strength of quadruple coil AMB in 2D

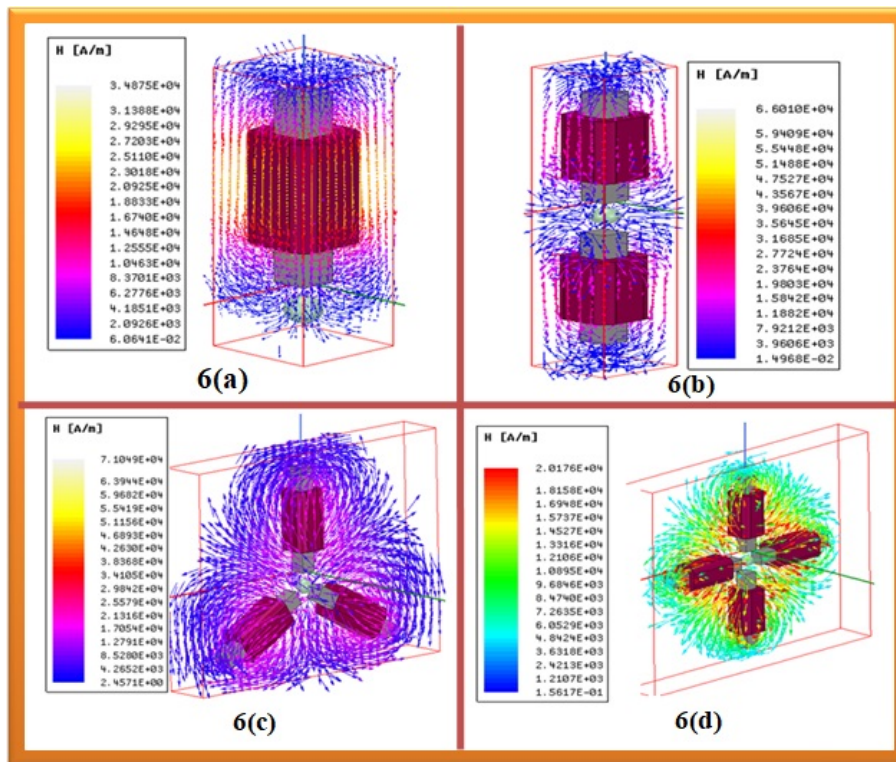


Figure 6: (a) Field strength of single coil AMB in 3D (b) Field strength of double coil AMB in 3D (c) Field strength of triple coil AMB in 3D (d) Field strength of quadruple coil AMB in 3D

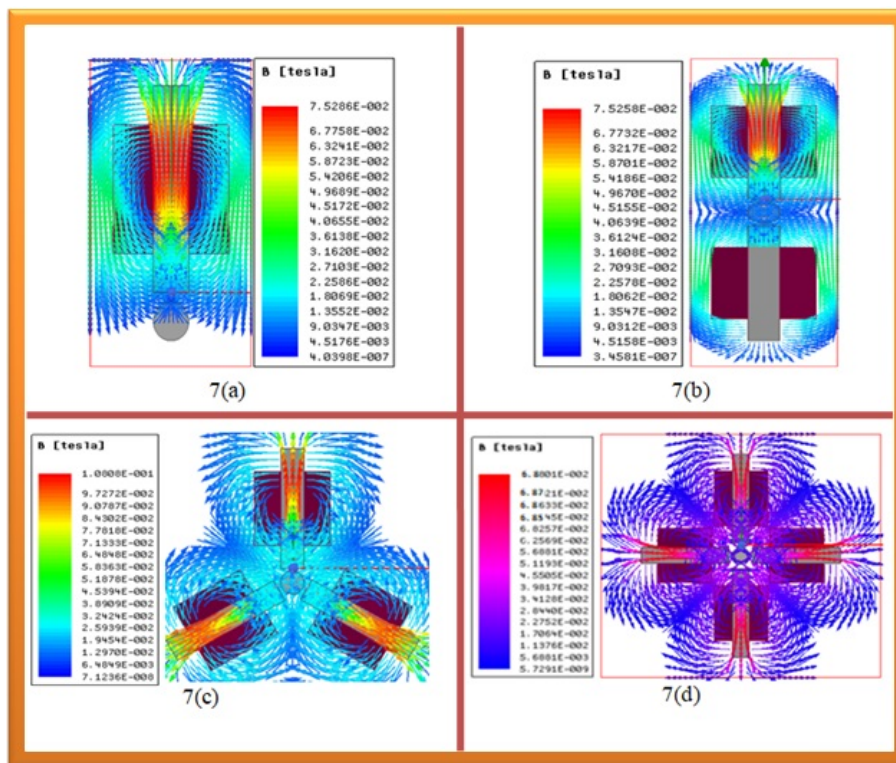


Figure 7: (a) Flux density of single coil AMB in 2D (b) Flux density of double coil AMB in 2D (c) Flux density of triple coil AMB in 2D (d) Flux density of quadruple coil AMB in 2D

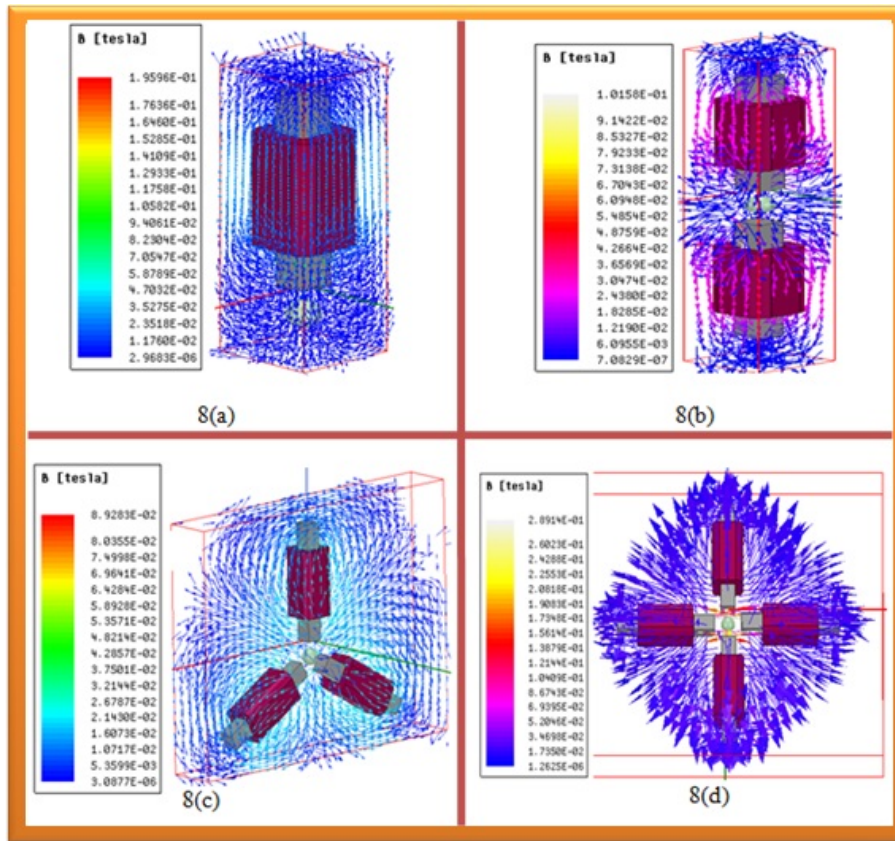


Figure 8: (a) Flux density of single coil AMB in 3D (b) Flux density of double coil AMB in 3D (c) Flux density of triple coil AMB in 3D (d) Flux density of quadruple coil AMB in 3D

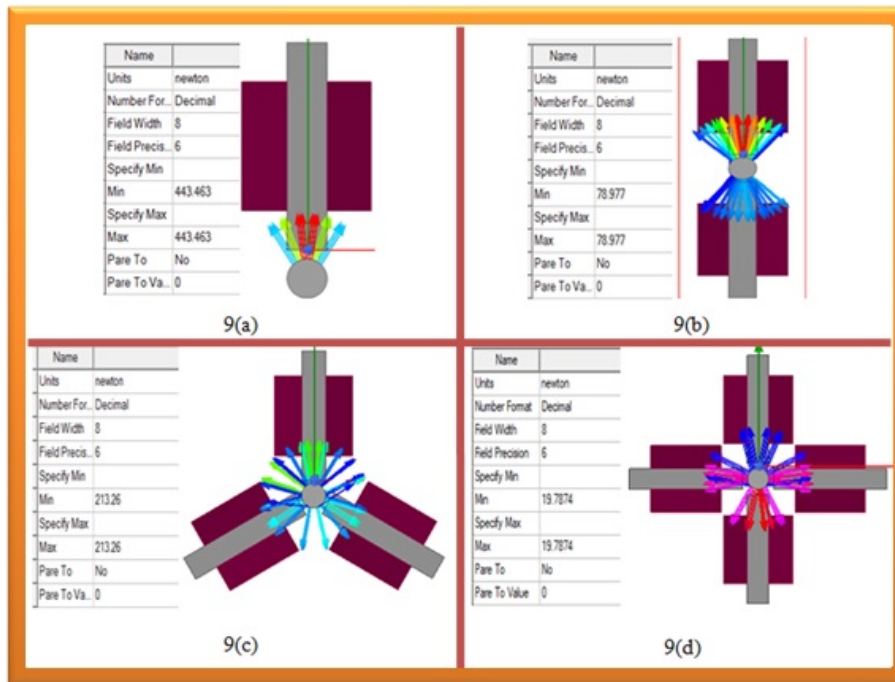


Figure 9: (a) Surface Force of single coil AMB in 2D (b) Surface Force of double coil AMB in 2D (c) Surface Force of triple coil AMB in 2D (d) Surface Force of quadruple coil AMB in 2D

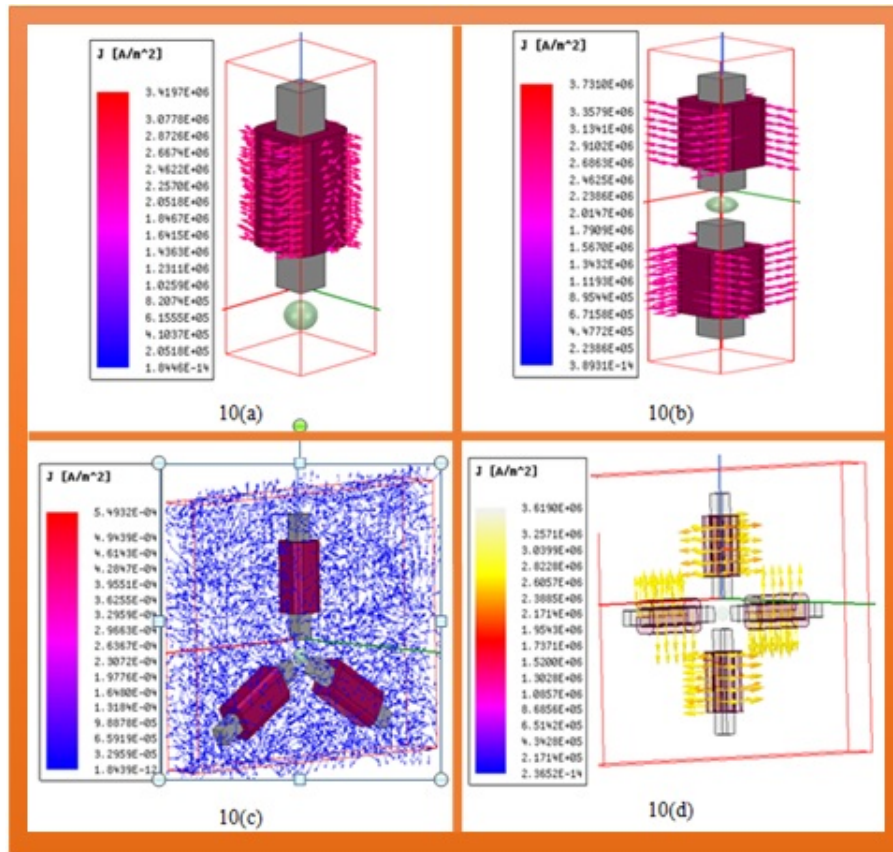


Figure 10: (a) Current density of single coil AMB in 3D (b) Current density of double coil AMB in 3D (c) Current density of triple coil AMB in 3D (d) Current density of quadruple coil AMB in 3D

#### 4 Analysis of the modeling result

Finite element analysis is done by using ANSYS Maxwell software for the I-type actuator to determine the flux line, magnetic field intensity, magnetic flux density, and force and inductance profile. Observed data for all these 2D and 3D analyses is tabulated in Table 4 and Table 5 respectively. Fig. 11 shows the characteristic graph for all 2D analyses and Fig. 12 shows the characteristic graph for 3D analyses. The inductance profiles for 2D and 3D are compared for all four types of actuator and plotted in Fig. 13. Due to the cancellation of force, inductance for single and triple coil greater than for the double and quadruple coil.

Fig. 14 shows a comparison of magnetic field strength in 2D and 3D for all four coils whereas a comparison of flux density is shown in Fig. 15.

All the parameters varied depending on the air gap between the actuator and rotor. Table 6 shows the analysis data of: flux pattern, field intensity, flux den-

Table 4: Magnetic analysis data of I-type actuator AMB in 2D for 10mm air gap

Actuator type	Field Strength	Flux Density	Current Density	Inductance
Single coil I-type	7.49E+048.26E-02	4.92E+06	41.247	
Double coil I-type	6.60E+045.1255E-02	3.72E+06	39.112	
Triple coil I-type	7.01E+049.93E-02	5.49E+06	41.326	
Quadruple coil I-type	4.02E+044.56E-02	3.62E+06	38.126	

sity, attraction force and inductance for single coil. The parameters change with the increase in air gap. The effect on parameters due to the change in air gap are plotted in 3D for single coil, double coils, triple coils and four coils.

A comparison between three parameters was made. The performance graph of the single coil for flux line

Table 5: Magnetic analysis data of I-type actuator AMB in 3D for 10mm air gap

Actuator type	Flux Line	Field Strength	Flux Density	Force
Single coil I-type	6.27E-04	2.51E+04	7.35E-02	443.769
Double coil I-type	5.37E-04	2.01E+04	6.0258E-02	78.769
Triple coil I-type	6.10E-04	3.29E+04	8.81E-02	213.26
Quadruple coil I-type	4.47E-04	2.04E+04	3.84E-02	19.78

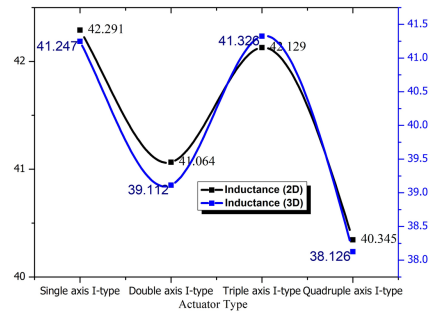


Figure 13: Comparison of inductance profiles for 2D and 3D analysis

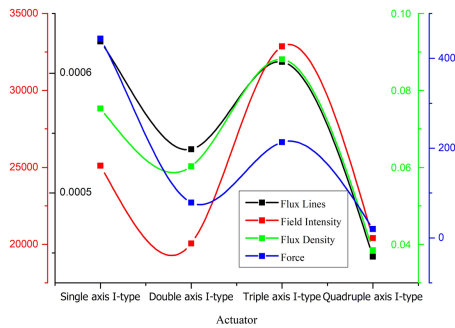


Figure 11: Characteristic graph of magnetic analysis for all parameters in 2D

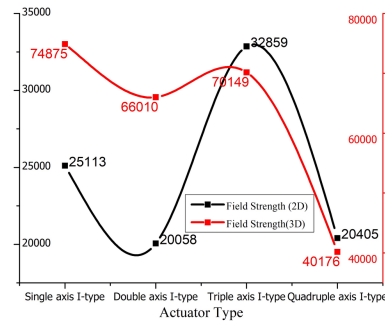


Figure 14: Comparison of magnetic field strength in 2D and 3D

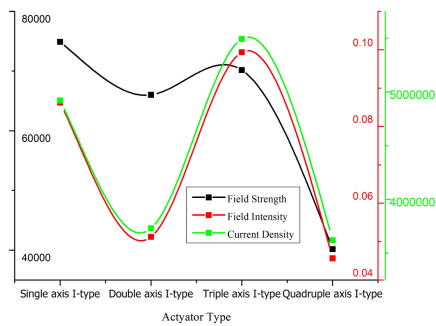


Figure 12: Characteristic graph of magnetic analysis for all parameters in 3D

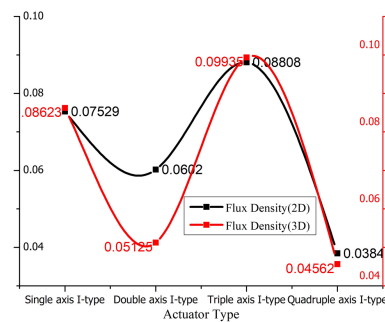


Figure 15: Comparison of flux density in 2D and 3D

and attraction force with the change in air gap is presented in Fig. 16, flux density, force and air gap are shown in Fig. 17, and field strength, force and air gap are shown in Fig. 18; similarly, for the double coil in Fig. 19, Fig. 20 and Fig. 21, for triple coils in Fig. 22, Fig. 23 and Fig. 24, and for quadruple coils in Figs. 25-27.

From these characteristics graphs it is observed that

when the air gap increases all the parameters decrease. These 3D graphs describe the behavior of the actuators.

Table 6: Magnetic analysis result of 2D single coil AMB

Air Gap	Flux Line	Field Strength	Flux Density	Force	Inductance
2	6.27E-04	2.51E+04	7.35E-02	297.3146	243
4	6.27E-04	2.51E+04	7.35E-02	241.5244	968
6	6.18E-04	2.50E+04	7.49E-02	178.5644	569
8	5.91E-04	2.41E+04	7.15E-02	125.7543	032
10	5.37E-04	2.07E+04	6.82E-02	42.29142	769
12	4.76E-04	1.70E+04	6.14E-02	32.36942	265
14	4.40E-04	1.41E+04	5.77E-02	26.46641	126
16	4.16E-04	1.15E+04	5.36E-02	17.59241	126
18	3.27E-04	9.57E+03	4.75E-02	5.234839	765
20	3.17E-04	9.17E+03	4.27E-02	0.764239	165

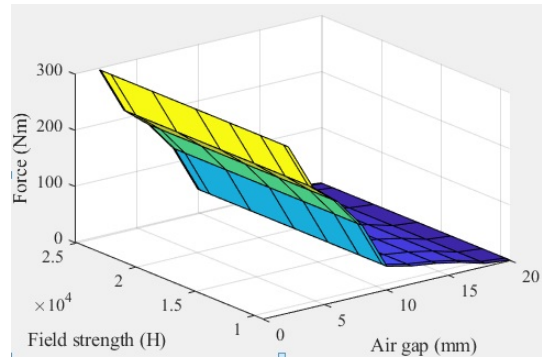


Figure 18: Field strength and attraction force with the change in air gap for single coil

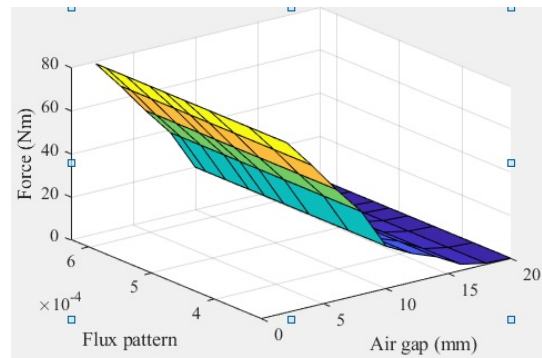


Figure 19: Flux line and attraction force with the change in air gap for double coil

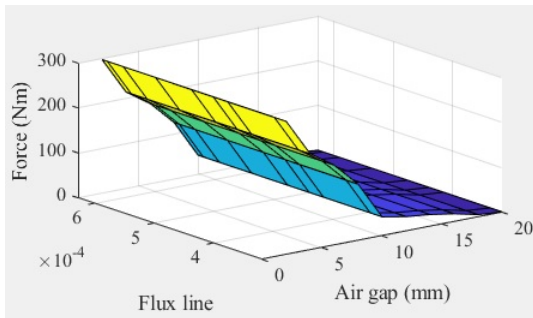


Figure 16: Flux line and attraction force with the change in air gap for single coil

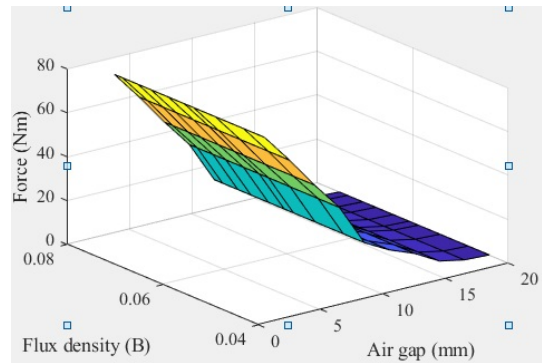


Figure 20: Flux density and attraction force with the change in air gap for double coil

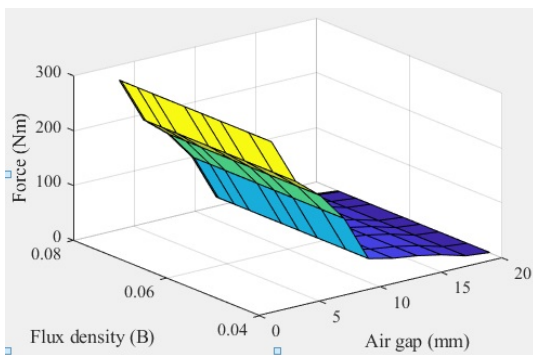


Figure 17: Flux density and attraction force with the change in air gap for single coil

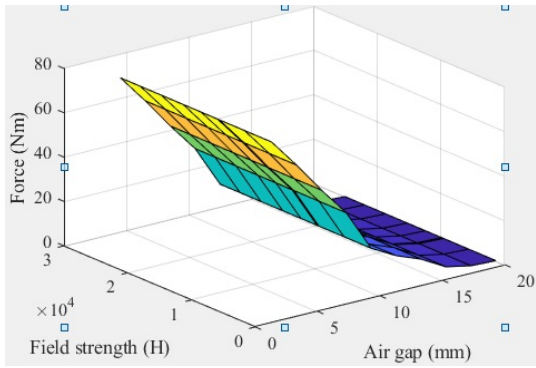


Figure 21: Field strength and attraction force with the change in air gap for double coil

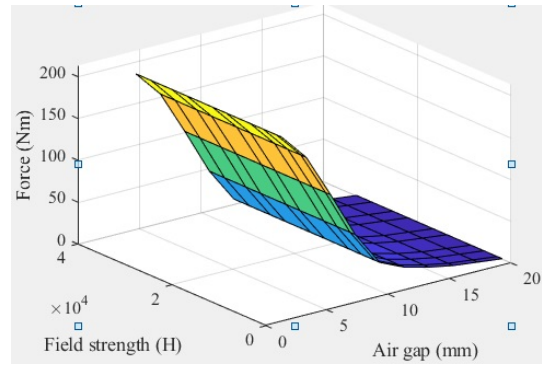


Figure 24: Field strength and attraction force with the change in air gap for triple coil

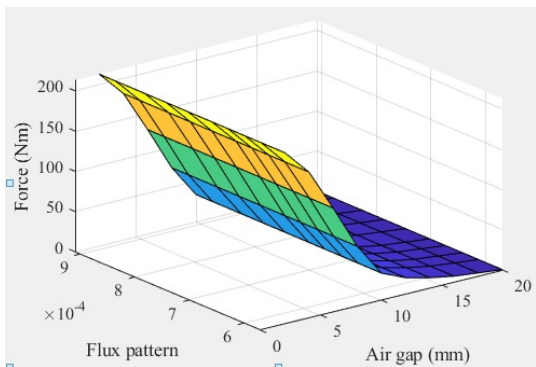


Figure 22: Flux line and attraction force with the change in air gap for triple coil

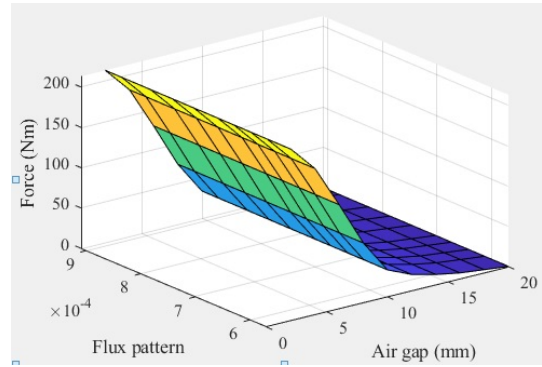


Figure 25: Flux pattern and attraction force with the change in air gap for quadruple coil

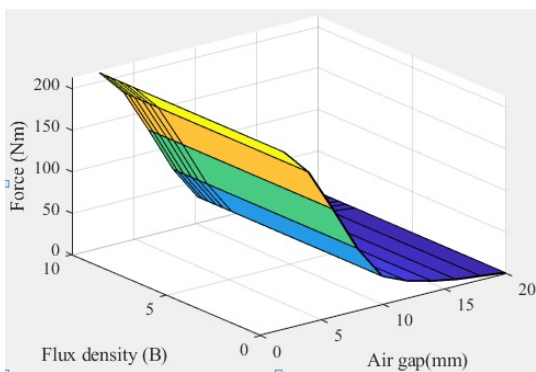


Figure 23: Flux density and attraction force with the change in air gap for triple coil

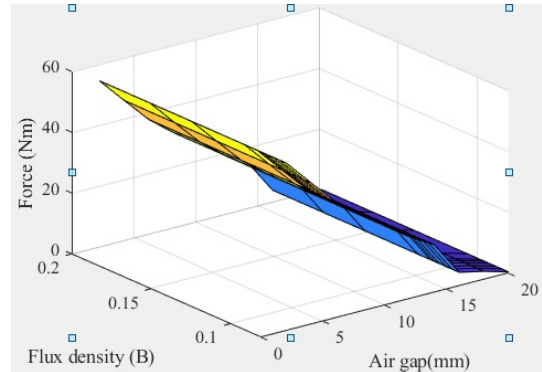


Figure 26: Flux density and attraction force with the change in air gap for quadruple coil

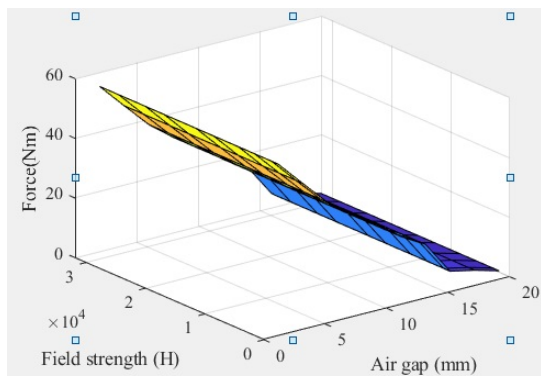


Figure 27: Field strength and attraction force with the change in air gap for quadruple coil

## 5 Conclusion

This manuscript presented the 2D and 3D magnetic analyses for single and multi-coil based actuators for the active magnetic bearing system. Analysis results are presented for 2D and 3D. To gain insight into the behavior of the actuators, single coil and multi-coils were compared for different quantities such as: flux lines, field intensity, field strength, force and inductance. Again a comparison between 2D and 3D was performed for field intensity, field strength and inductance profile. From this comparative magnetic analysis it is observed that force and other parameters differ depending on the number of coils. Here force is greater for single coil and triple coil because there is no opposite cancellation force, whereas force is less for the double coil and four coil due to opposite cancellation force. For better observation comparative analysis is done by factoring in three quantities, as plotted in a 3D graph. These comparative analyses will help to choose a suitable actuator for the purpose of delivering better Active Magnetic Bearing system design.

## References

1. Banerjee, S., Sarkar, M.K., and Chakraborty, C. (2013) Analysis design, fabrication and testing of three actuators based electromagnetic levitation system for vehicle applications. *IECON 2013 - 39th Annual Conference of the IEEE Industrial Electronics Society*.
2. Raghunathan, P., and Logashanmugam, E. (2016) Design and testing of electromagnetic actuator used in axial active magnetic bearing. *2016 International Conference on Control Instrumentation, Communication and Computational Technologies (ICCICT)*.
3. Debnath, S., Biswas, P.K., and Laldingliana, J. (2017) Analysis and simulation of PWM based power amplifier for single axis Active Magnetic Bearing (AMB). *2017 IEEE Transportation Electrification Conference (ITEC-India)*.
4. Laldingliana, J., Debnath, S., and Biswas, P.K. (2018) Analysis of a Single Actuator Double Winding Active Magnetic Bearing (AMB) Using Ansys Maxwell Simulation Software. *2018 2nd International Conference on Power Energy and Environment: Towards Smart Technology (ICEPE)*.
5. (2019) Fem Software Based 2-D and 3-D Construction and Simulation of Single and Double Coils Active Magnetic Bearing. *International Journal of Innovative Technology and Exploring Engineering*, **8** (11),

665–675.

6. Wajnert, D. (2013) Comparison of magnetic field parameters obtained from 2D and 3D finite element analysis for an active magnetic bearing. *2013 International Symposium on Electrodynamics and Mechatronic Systems (SELM)*.
7. You, J., Wang, R., Chen, H., Chen, F., and Liang, H. (2017) A novel design of the rotary electromagnetic actuator and the analysis of critical demagnetization state for its permanent magnet. *2017 IEEE International Magnetism Conference (INTERMAG)*.
8. (1994) *Active Magnetic Bearings: Basics, Properties and Applications of Magnetic Bearings*, vdf Hochschulverlag AG, an der ETH Zurich.
9. Review Lecture - Electromagnetic suspension and levitation techniques — Proceedings of the Royal Society of London. A. Mathematical and Physical Sciences.
10. Debnath, S., and Biswas, P.K. (2020) Design analysis, and testing of I-type electromagnetic actuator used in single-coil active magnetic bearing. *Electrical Engineering*.
11. (2009) *Magnetic bearings: Theory, design, and application to rotating machinery*, Springer.
12. Schofield, N., Lonsdale, A., and Hodges, A.Y. (2004) Static and Dynamic Electromagnetic Actuator Designs for a Fluctuating Force Module (FFM) Calibration Test Facility. *IEEE Transactions on Magnetics*, **40** (4), 2074–2076.
13. Lim, S., and Min, S. (2012) Design Optimization of Permanent Magnet Actuator Using Multi-Phase Level-Set Model. *IEEE Transactions on Magnetics*, **48** (4), 1641–1644.
14. Safaeian, R., and Heydari, H. (2018) Comprehensive comparison of different structures of passive permanent magnet bearings. *IET Electric Power Applications*, **12** (2), 179–187.
15. Wang, D., Wang, N., Ye, C., and Chen, K. (2017) Research on analytical bearing capacity model of active magnetic bearings based on magnetic saturation. *IET Electric Power Applications*, **11** (9), 1548–1557.
16. Lenka, V.R., and Kakoty, S.K. (2014) Design of compact active magnetic bearing. *International Journal of Applied Sciences and Engineering Research*, **3**.